Journal of Quantitative Spectroscopy & Radiative Transfer 112 (2011) 163–173

Contents lists available at ScienceDirect

Journal of Quantitative Spectroscopy & Radiative Transfer

journal homepage: www.elsevier.com/locate/jqsrt

Diffraction and external reflection by dielectric faceted particles

Lei Bi [a,*], Ping Yang [b], George W. Kattawar [a], Yongxiang Hu [c], Bryan A. Baum [d]

[a] Department of Physics, Texas A&M University, College Station, TX 77843, USA
[b] Department of Atmospheric Sciences, Texas A&M University, College Station, TX 77843, USA
[c] NASA Langley Research Center, Hampton, VA 23681, USA
[d] Space Science and Engineering Center, University of Wisconsin-Madison, 1225 West Dayton St., Madison, WI 53706, USA

ARTICLE INFO

Article history:
Received 14 December 2009
Received in revised form
11 February 2010
Accepted 17 February 2010

Keywords:
Diffraction
External reflection
Scattering
Hexagonal ice crystal

ABSTRACT

The scattering of light by dielectric particles much larger than the wavelength of incident light is attributed to diffraction, external reflection and outgoing refracted waves. This paper focuses on diffraction and external reflection by faceted particles, which can be calculated semi-analytically based on physical optics. Three approximate methods; the surface-integral method (SIM), the volume-integral method (VIM), and the diffraction plus reflection pattern from ray optics (DPR) are compared. Four elements of the amplitude scattering matrix in the SIM and the VIM are presented in an explicit form. Of interest is that diffraction and external reflection are separable in the SIM, whereas they are combined in the VIM. A feature of zero forward reflection is noticed in the SIM. The applicability of the DPR method is restricted to particles with random orientations. In the manner of van de Hulst, we develop a new technique to compute the reflection pattern of randomly oriented convex particles using spheres with the same refractive index, resulting in an improvement in the precision of the reflection calculation in near-forward and near-backward directions. The accuracy of the aforementioned three methods is investigated by comparing their results with those from the discrete-dipole-approximation (DDA) method for hexagonal particles at the refractive index of 1.3+i1.0. For particles with fixed orientations, it is found that the SIM and the VIM are comparable in accuracy and applicable when the size parameter is on the order of 20. The ray-spreading effect on the phase function is evident from the results of various size parameters. For randomly oriented particles, the DPR is more efficient than the SIM and the VIM.

1. Introduction

In the context of physical optics, the scattering of light by dielectric particles much larger than the wavelength of the incident light is attributed to three components: diffraction, external reflection, and outgoing refracted waves [1,2]. Traditionally, the ray-tracing technique, based on geometric optics, is used to compute the electric fields associated with reflected and refracted rays, and the Fraunhofer diffraction theory is employed to account for the wave nature of light [3–7]. The conventional geometric optics method (CGOM) is conceptually simple but is only valid for particles where the size parameter χ is much greater than 20 ($\chi=2\pi d/\lambda$, where d is the characteristic dimension of the particle and λ is the wavelength). To improve the accuracy of the CGOM, especially for moderate sized particles ($\chi\sim50$), several methods of combining exact electromagnetic integral equations and geometric optics have been developed in [8–10]. In these methods, the near field is approximated in terms of the solution from the geometric optics method, and the far field in the radiation zone is obtained by mapping the

* Corresponding author. Tel.: +1 979 862 1722.
E-mail address: bilei@tamu.edu (L. Bi).

0022-4073/$ - see front matter © 2010 Elsevier Ltd. All rights reserved.
doi:10.1016/j.jqsrt.2010.02.007

near field via either a surface-integral [8,9] or a volume-integral equation [10]. However, this exact transformation procedure has been demonstrated to be computationally ineffective, particularly for randomly oriented particles. To overcome the computational difficulty, Yang and Liou proposed a simplified mapping technique that incorporates the so-called ray spreading effect into the phase matrix simulated from the CGOM [9], a polarized diffraction matrix to replace the scalar Fraunhofer diffraction [11], and a ray-by-ray algorithm to calculate the efficiency factors [10]. This simplified approach (hereafter, the improved geometric optics method, IGOM), has been used to solve the single-scattering properties of randomly oriented ice crystals and dust aerosols in the atmosphere [12–17]. For particles that have parallel planar faces, such as a hexagonal plate or column, the delta-transmission term [18–19] in the phase function was removed. The basic IGOM formalism was reported by Yang and Liou [20]. Note that there are also other modifications of the geometric optics method. Borovoi and Grishin [21] discussed the method of tracing the plane-parallel outgoing beams instead of rays in the near-field simulations of hexagonal ice crystals. A method that combines the ray tracing calculation and the concept of energy flow lines to model the diffraction effect was reported by Hess et al. [22], Clarke et al. [23], and Hess [24].

The intent of this study is to investigate the efficiency and accuracy of the calculations of diffraction and external reflection for faceted particles such as those found in ice clouds. The calculation of external reflection from faceted particles is quite different from that of spherical particles with smooth surfaces. In the case of spheres, the agreement between the external reflection pattern calculated from geometric rays and that from zero-order Debye series [25] or from the Lorenz–Mie theory for strong absorbing particles is excellent at larger scattering angles [26]. A detailed treatment of the diffraction and external reflection associated with an arbitrarily oriented spheroid was discussed by Lock [27]. For a faceted particle, singularity points exist in the reflection pattern when the particle is at a fixed orientation in the context of ray optics. Therefore, ray optics is normally applied to randomly oriented faceted particles.

Specifically, we intend to show that the first-order scattering for faceted particles can be derived semi-analytically from a surface-integral equation [9] or a volume-integral equation [26]. This is the main reason why diffraction and external reflection of light are investigated separately from the refracted waves. In [9] and [26], an amplitude scattering matrix is represented as a product of several matrices in conjunction with some local coordinate systems. Four elements in the amplitude scattering matrix can be derived explicitly as functions of the direction of the incident light, the normal direction of local surface and the refractive index. Although the surface-integral and volume-integral transformations of the near field to the far field are equivalent, the formulae associated with diffraction and external reflection derived from the two integral equations are not exactly the same. To our best knowledge, this feature has not been investigated in previous studies and a comparison of the accuracy of the two methods has not been reported in the literature.

Furthermore, we notice that the traditional method of using the shadow diffraction theory and the ray-tracing technique to calculate the diffraction and reflection by randomly oriented particles can be improved. van de Hulst [1] suggests that the normalized reflection pattern for randomly oriented convex particles should be the same as that for spheres with the same surface conditions. Therefore, the reflection pattern for a sphere can be used to replace that calculated for general convex particles. This treatment will remove the difficulty in determining the scattered energy within the solid angle elements near the forward and backward directions.

The accuracy of the aforementioned three methods can be examined in the cases of highly absorptive particles by employing exact numerical scattering methods, such as the finite-difference time domain (FDTD) method [28–30], the discrete dipole approximation (DDA) method [31–34], and the T-matrix method [35–38]. In principle, the diffraction and external reflection cannot be separated from the complete solution in the exact numerical methods. In practice, we assume that the contribution to the scattering phase matrix from the refracted waves can be neglected for highly absorbing particles. Therefore, it is possible to determine the accuracy of the first-order scattering solution, and to develop the most accurate and efficient numerical algorithm for the IGOM.

The remainder of this paper is organized as follows. Section 2 describes three feasible methods for calculating the diffraction and external reflection: the surface integral method (SIM), the volume integral method (VIM), and the method of diffraction plus external reflection from ray optics (DPR). In Section 3, we compare the phase functions simulated from these methods for hexagonal particles. The accuracy of these methods is examined in comparison with their counterparts from the DDA method for hexagonal particles with strong absorption. The conclusions of this study are given in Section 4.

2. Computational methods

2.1. Surface integral method

The electric field in the radiation zone can be formulated in terms of the Kirchhoff surface integral over the near field [9,39] as follows:

$$\vec{E}^{s}(\vec{r})|_{kr\to\infty} = \frac{\exp(ikr)}{-ikr}\frac{k^2}{4\pi}\hat{r}\times\oint\!\!\!\oint_{s}\{\hat{n}_s\times\vec{E}(\vec{r}\,') - \hat{r}\times[\hat{n}_s\times\vec{H}(\vec{r}\,')]\}\exp(-ik\hat{r}\cdot\vec{r}\,')d^2\vec{r}\,', \quad (1)$$

where k is the wave number, $\hat{r}$ is the scattering direction to observation position, s is the particle surface or any surface which encloses the particle and $\hat{n}_s$ is the outward pointing unit vector normal to the surface s. E and H can be either the scattered field or the total field on the surface. Note that the integral in Eq. (1) is a linear operator with respect to the electric and magnetic fields. Therefore, the contribution of external reflection to the far field can be calculated separately by mapping the

reflected field on the illuminated side of the particle. The contribution from diffraction can be computed by mapping the incident field on the illuminated side or minus the incident field on the unilluminated side of the particle.

The amplitude scattering matrix can be written as the sum of two parts:

$$S = S^r + S^d, \tag{2}$$

where S^d and S^r are the 2×2 amplitude scattering matrix associated with diffraction and external reflection, respectively. For a local planar surface, the sum of S^d and S^r can be written as

$$S = D(\tilde{S}^r + \tilde{S}^d), \tag{3}$$

where D is an integral over the local surface, given by

$$D = \frac{k^2}{4\pi}\int_s \exp\left\{ik(\hat{e}^i - \hat{r})\cdot\vec{r}'\right\} d^2\vec{r}'. \tag{4}$$

In Eq. (4), $\hat{e}^i$ is the direction of incident wave. The expressions of four elements of $\tilde{S}_d$ and $\tilde{S}_r$ in Eq. (3) can be explicitly obtained as follows:

$$\tilde{S}^d_{11} = (1+\cos\theta)\cos\theta_i - \sin\theta\sin\theta_i\sin\phi_0, \tag{5}$$

$$\tilde{S}^d_{12} = \sin\theta\sin\theta_i\cos\phi_0, \tag{6}$$

$$\tilde{S}^d_{21} = -\tilde{S}^d_{12}, \tag{7}$$

$$\tilde{S}^d_{22} = \tilde{S}^d_{11}, \tag{8}$$

$$\tilde{S}^r_{11} = (1-\cos\theta)\cos\theta_i(-R_\alpha\sin^2\phi_0 + R_\beta\cos^2\phi_0) - R_\alpha\sin\theta\sin\theta_i\sin\phi_0, \tag{9}$$

$$\tilde{S}^r_{12} = (1-\cos\theta)\cos\theta_i(R_\alpha + R_\beta)\sin\phi_0\cos\phi_0 + R_\alpha\sin\theta\sin\theta_i\cos\phi_0, \tag{10}$$

$$\tilde{S}^r_{21} = -(1-\cos\theta)\cos\theta_i(R_\alpha + R_\beta)\sin\phi_0\cos\phi_0 - R_\beta\sin\theta\sin\theta_i\cos\phi_0, \tag{11}$$

$$\tilde{S}^r_{22} = (1-\cos\theta)\cos\theta_i(R_\alpha\cos^2\phi_0 - R_\beta\sin^2\phi_0) - R_\beta\sin\theta\sin\theta_i\sin\phi_0, \tag{12}$$

where θ_i is the incident angle, θ is the scattering angle, ϕ_0 is the angle between the scattering plane and a polarization vector β_1 as shown in Fig. 1. R_α and R_β are the Fresnel reflection coefficients corresponding to the parallel and perpendicular components of the electric vector with respect to the incident plane. Note that $\tilde{S}^r$ and $\tilde{S}^d$ are related to the normal direction of the planar surface, and D is a shape factor determined by the boundary shape and size of the local planar surface. The obvious optics information contained in the shape factor in Eq. (3) is that D tends to be largest when the observational direction is aligned with the reflected ray or the incident direction, which is partly responsible for the peaks associated with diffraction and external reflection in the phase function. The shape factor for hexagonal particles was reported in a previous study [26]. For arbitrarily shaped local planar surface, the algorithm for calculating the shape factor is discussed in Appendix A. The illuminated side of the particle is usually composed of N local planar surfaces. The amplitude scattering matrix is given as follows:

$$S = \sum_{i=1}^{N} D_i(\tilde{S}^d_i + \tilde{S}^r_i), \tag{13}$$

where D_i, $\tilde{S}^d_i$, and $\tilde{S}^r_i$ corresponds to D, $\tilde{S}^d$, and $\tilde{S}^r$ at the ith surface.

The formula (13) is not exact due to the approximation of the reflected field near the edges of the planar surfaces. It is expected that the inaccuracy of the reflected field near the edge tends to be small when the size of the particle is large, as ray optics is accurate when the dimension of the particle face is much larger than the incident wavelength. The accuracy of this approximation to the solution in the far field will be discussed in Section 3.

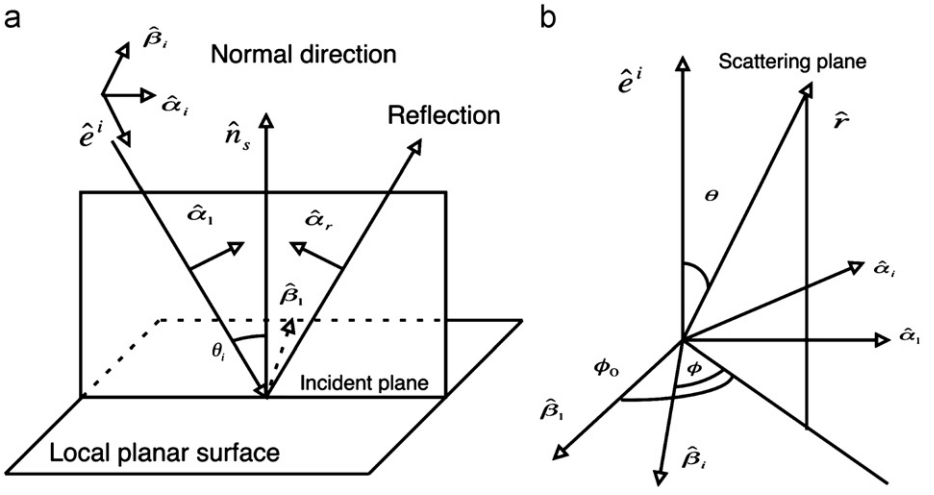

Fig. 1. Illustration of coordinate systems associated with reflection. (a) The local coordinate system $(\hat{\beta}_1, \hat{\alpha}_1, \hat{e}_i)$ of the incident ray is rotated to $(\hat{\beta}_1, \hat{\alpha}_1, \hat{e}_i)$ in order that the Fresnel coefficients can be employed to calculate the reflected electric-magnetic field vectors parallel and perpendicular to the incident plane. (b) θ is the scattering angle, ϕ is the azimuthal angle of scattering plane, and ϕ_0 is the angle between $\hat{\beta}_1$ and the scattering plane.

The diffraction calculation is generally not exactly the same as that from Babinet's principle [1] stating that the distribution of diffracted intensity by a 3-D solid particle is identical to that by an aperture with the same shape and size of the particle's geometric projection. In the context of the Kirchhoff surface integral, diffraction comes from the integration of incident field on the illuminated side of the particle or minus incident field on the un-illuminated side. Note that the integration of incident fields over a closed surface is zero. It is found that the integration of the incident field in terms of the illuminated side differs from the integration of minus the incident field in terms of the projection except for some special cases. As an example, we investigate the diffraction by a regular hexahedron. Let the direction of the incident wave be perpendicular to one of the faces. In this case, the amplitude scattering matrices associated with the bottom, the top and the geometric projection are different by a phase factor (referred to Appendix B). Therefore, the elements of the phase matrix are exactly the same as expected from Babinet's principle. For other orientations of the regular hexahedron, phase matrix elements from the SIM and Babinet's principle are different. Similarly, the SIM and Babinet's principle give the same result of phase matrix for spheres, but different results for ellipsoids because the boundary that separates the illuminated side and un-illuminated side is not perpendicular to the incident direction except for some special cases when the incident directions aligned with the three principle axes. In a general case, inconsistency exists between Babinet's principle and the present formulation of diffraction when the differences of amplitude scattering matrices derived from the two methods cannot be accounted for by a phase factor. Fig. 2 shows the comparison of the distribution of diffracted intensity by a cube computed from the present method and that from Babinet's principle. As shown in Fig. 2, the difference between results from the two methods is very small near the forward scattering direction. Note that the two methods yield the same results in the exact forward direction.

2.2. Volume integral method

The far field can be formulated as a volume integral over the internal field within the particle [10,40]:

$$\vec{E}^{s}(\vec{r})|_{kr\to\infty}=\frac{k^2\exp(ikr)}{4\pi r}\int(m^2-1)\left\{\vec{E}(\vec{r}')-\hat{r}\left[\hat{r}\cdot\vec{E}(\vec{r}')\right]\right\}\times\exp(-ik\hat{r}\cdot\vec{r}')d^3\vec{r}', \tag{14}$$

where m is the refractive index. The amplitude scattering matrix associated with the diffraction and external reflection implied in this equation has been reported in Yang et al. [26] and formulated in terms of a product of the matrices associated with several coordinate system transformations. The explicit elements of the amplitude scattering matrix were obtained in this study as follows:

$$\begin{bmatrix} S_{11} & S_{12} \\ S_{21} & S_{22} \end{bmatrix}=\sum_{i=1}^{N} D_i\frac{(m^2-1)\cos\theta_t}{N_r+iN_i-\hat{r}\cdot\hat{e}_t}\begin{bmatrix} \tilde{S}_{11} & \tilde{S}_{12} \\ \tilde{S}_{21} & \tilde{S}_{22} \end{bmatrix}, \tag{15}$$

where N_r+iN_i is the effective complex refractive index [26], θ_t is the angle of refraction (different for each local planar surface), and $\hat{e}_t$ is the propagation direction of the first-order refracted wave. Four elements of the matrix $\tilde{S}$ are in the form,

$$\tilde{S}_{11}=[T_\alpha\cos(\theta_i-\theta_t)\sin^2\phi_0+T_\beta\cos^2\phi_0-T_\gamma\sin(\theta_i-\theta_t)\sin^2\phi_0]\cos\theta-[T_\alpha\sin(\theta_i-\theta_t)+T_\gamma\cos(\theta_i-\theta_t)]\sin\theta\sin\phi_0, \tag{16}$$

$$\tilde{S}_{12}=[-T_\alpha\cos(\theta_i-\theta_t)+T_\beta+T_\gamma\sin(\theta_i-\theta_t)]\cos\theta\cos\phi_0\sin\phi_0-[T_\alpha\sin(\theta_i-\theta_t)+T_\gamma\cos(\theta_i-\theta_t)]\sin\theta\cos\phi_0, \tag{17}$$

$$\tilde{S}_{21}=[-T_\alpha\cos(\theta_i-\theta_t)+T_\beta+T_\gamma\sin(\theta_i-\theta_t)]\cos\phi_0\sin\phi_0, \tag{18}$$

$$\tilde{S}_{22}=T_\alpha\cos(\theta_i-\theta_t)\cos^2\phi_0+T_\beta\sin^2\phi_0-T_\gamma\sin(\theta_i-\theta_t)\cos^2\phi_0, \tag{19}$$

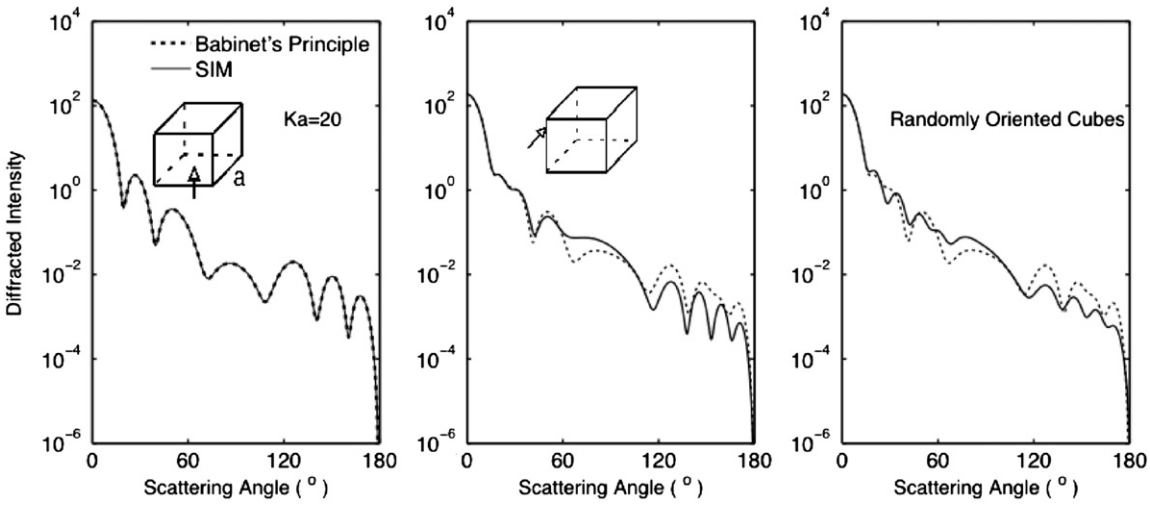

Fig. 2. Distribution of diffracted intensity for cubes computed from the present SIM method (integration over illuminated side) and Babinet's principle (integration over the particle projection). The results are averaged over scattering azimuthal angles.

where θ_i is the angle of incidence; T_α, T_β, and T_γ are three transmission coefficients [26], given by

$$T_\alpha = \frac{2(N_r + iN_i)\cos\theta_i}{m^2\cos\theta_i + [N_r\cos\theta_t + iN_i/\cos\theta_t]}, \tag{20}$$

$$T_\beta = \frac{2\cos\theta_i}{\cos\theta_i + [N_r\cos\theta_t + iN_i/\cos\theta_t]}, \tag{21}$$

$$T_\gamma = \frac{i2N_i\tan\theta_t\cos\theta_i}{m^2\cos\theta_i + [N_r\cos\theta_t + iN_i/\cos\theta_t]}. \tag{22}$$

The formulation of the three transmission coefficients, taking into account the effect of inhomogeneous waves for absorptive particles, has been reported by Yang et al. [26].

Eqs. (1) and (14) are equivalent when the near field is exactly known. However, the amplitude scattering matrices associated with the diffraction and the external reflection derived are not exactly equivalent. Of interest is that the diffraction and the external reflection are inherently combined in Eq. (15). A comparison of numerical results from the SIM and the VIM will be given in Section 3.

2.3. Shadow diffraction and reflection from ray optics

The DPR method is only applicable to randomly oriented particles due to singularity points existing in the phase function. In the DPR method, the amplitude scattering matrix associated with diffraction is represented in terms of an integral over either the projection or the illuminated side of the particle. The reflection is calculated through geometric optics based on the ray-tracing technique. The energy associated with diffraction is assumed to be one half of the extinction cross section. The final phase matrix is given by

$$P = w_d P^d + w_r P^r, \tag{23}$$

where P^d and P^r are normalized phase matrices associated with diffraction and external reflection, respectively. w_d and w_r in (23) are relative weights, given by

$$w_d = \sigma_e/(\sigma_e + 2\sigma_r), \tag{24}$$

$$w_r = 2\sigma_r/(\sigma_e + 2\sigma_r), \tag{25}$$

where σ_r and σ_e are the cross sections associated with the reflection and extinction calculated from the ray-tracing technique. P^d is calculated from the Fraunhofer diffraction theory as follows:

$$P^d = \begin{bmatrix} |S_{11}^d|^2 + |S_{22}^d|^2 & |S_{22}^d|^2 - |S_{11}^d|^2 & 0 & 0 \\ |S_{22}^d|^2 - |S_{11}^d|^2 & |S_{11}^d|^2 + |S_{22}^d|^2 & 0 & 0 \\ 0 & 0 & 2\mathrm{Re}(S_{11}^{d*}S_{22}^d) & 2\mathrm{Im}(S_{11}^d S_{22}^{d*}) \\ 0 & 0 & -2\mathrm{Im}(S_{11}^d S_{22}^{d*}) & 2\mathrm{Re}(S_{11}^{d*}S_{22}^d) \end{bmatrix}, \tag{26}$$

where the two diagonal elements of the amplitude scattering matrix are given by [11]

$$S_{11}^d = D(1+\cos\theta)\cos\theta, \tag{27}$$

$$S_{22}^d = D(1+\cos\theta). \tag{28}$$

P^r is related to the Fresnel reflection coefficients, given by

$$P^r = \begin{bmatrix} R_\alpha R_\alpha^* + R_\beta R_\beta^* & R_\alpha R_\alpha^* - R_\beta R_\beta^* & 0 & 0 \\ R_\alpha R_\alpha^* - R_\beta R_\beta^* & R_\alpha R_\alpha^* + R_\beta R_\beta^* & 0 & 0 \\ 0 & 0 & 2\mathrm{Re}(R_\alpha R_\beta^*) & 2\mathrm{Im}(R_\alpha R_\beta^*) \\ 0 & 0 & -2\mathrm{Im}(R_\alpha R_\beta^*) & 2\mathrm{Re}(R_\alpha R_\beta^*) \end{bmatrix} \times \begin{bmatrix} 1 & 0 & 0 & 0 \\ 0 & \cos(\phi_0-\phi) & \sin(\phi_0-\phi) & 0 \\ 0 & -\sin(\phi_0-\phi) & \cos(\phi_0-\phi) & 0 \\ 0 & 0 & 0 & 1 \end{bmatrix}. \tag{29}$$

Note that for large randomly oriented convex particles, the reflection pattern is the same as that for spheres with the same surface area and refractive index, as articulated by van de Hulst [1]. Therefore, it is not necessary to compute the reflection pattern by using the ray-tracing technique, but the reflection pattern can be computed with the analytical solution for spheres [26], given by

$$P_{11}^r(\theta) = c\left|R_\alpha\left(\frac{\pi-\theta}{2}\right)\right|^2 + \left|R_\beta\left(\frac{\pi-\theta}{2}\right)\right|^2, \tag{30}$$

where c is normalization constant, and || indicates the modulus of a complex quantity.

3. Results and discussion

In this section, we present the optical properties of hexagonal particles simulated from the SIM, the VIM and the DPR methods, and estimate their applicability and accuracy. For some selected simulations, a comparison between the aforementioned approximate results and those from the DDA method is presented. The ADDA code used in this study was developed by Yurkin and Hoekstra [34]. The refractive index is selected to be 1.3+i1.0 for the present simulations. To minimize the contribution from refracted waves, a proper selection of the imaginary part of the refractive index depends on the size parameter. The smaller the size parameter, the larger the imaginary part of the refractive index required. A large imaginary part of the refractive index can also increase the computational efficiency of the DDA method. Therefore, in this study the imaginary part of refractive index is selected to be 1.0. For the ADDA simulations, number of dipoles per wavelength is assumed to be 16.4 according to the rule of thumb [34] and the required relative residual norm is specified as 1×10^{-5} for the involved bi-conjugate gradient solver.

The SIM and the VIM are applicable to particles with fixed orientations. Figs. 3–5 compare the phase functions of compact hexagonal particles (i.e., the aspect ratio is unity) simulated from the SIM, the VIM and the DDA for three representative orientations. For each orientation, simulations were carried out at three size parameters: 20, 50 and 100 (i.e., small, moderate, and large values of the size parameter) and phase function is averaged over scattering planes. In Fig. 3, the direction of the incident light is aligned with the axis of six-fold symmetry. A continuous pattern is obtained from the SIM and the VIM. As seen from the figure, the overall pattern of the phase functions from the SIM and the VIM agree with those from the ADDA. Large differences are found at scattering angles

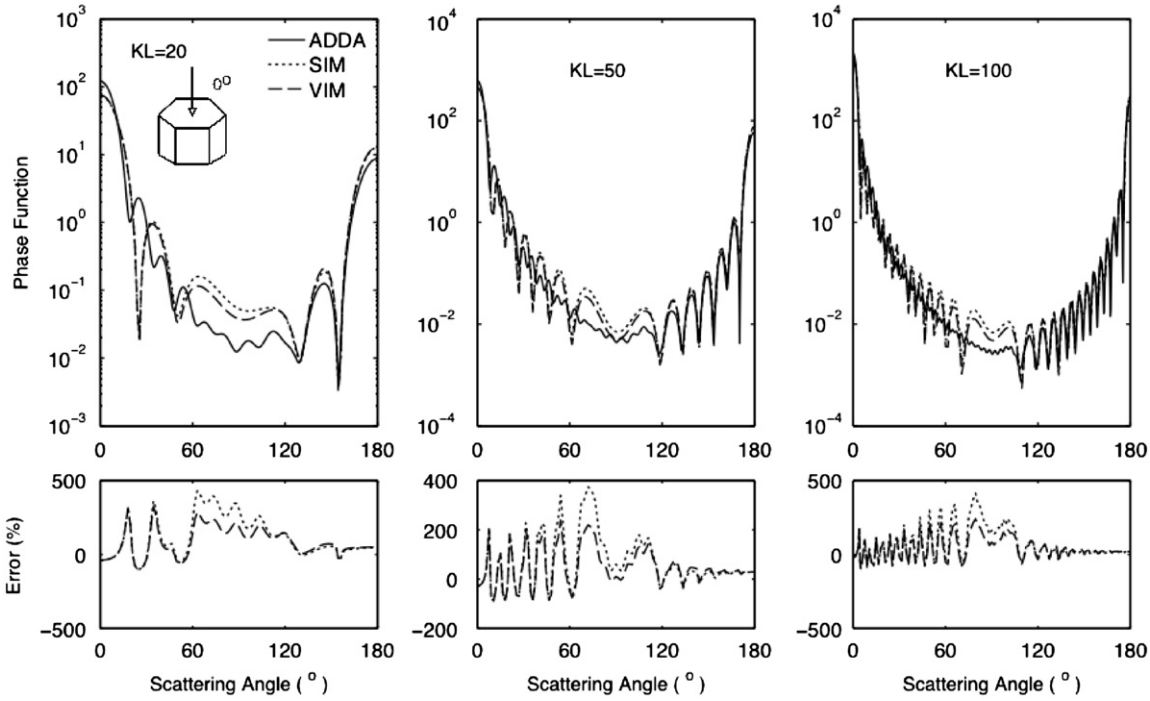

Fig. 3. Phase functions for hexagonal particles. The direction of the incident light is aligned with the axis of six-fold symmetry. The refractive index is 1.3+i1.0. The lower panel shows the relative differences between the results from the SIM and the VIM and that from the ADDA. The results are averaged over scattering azimuthal angles.

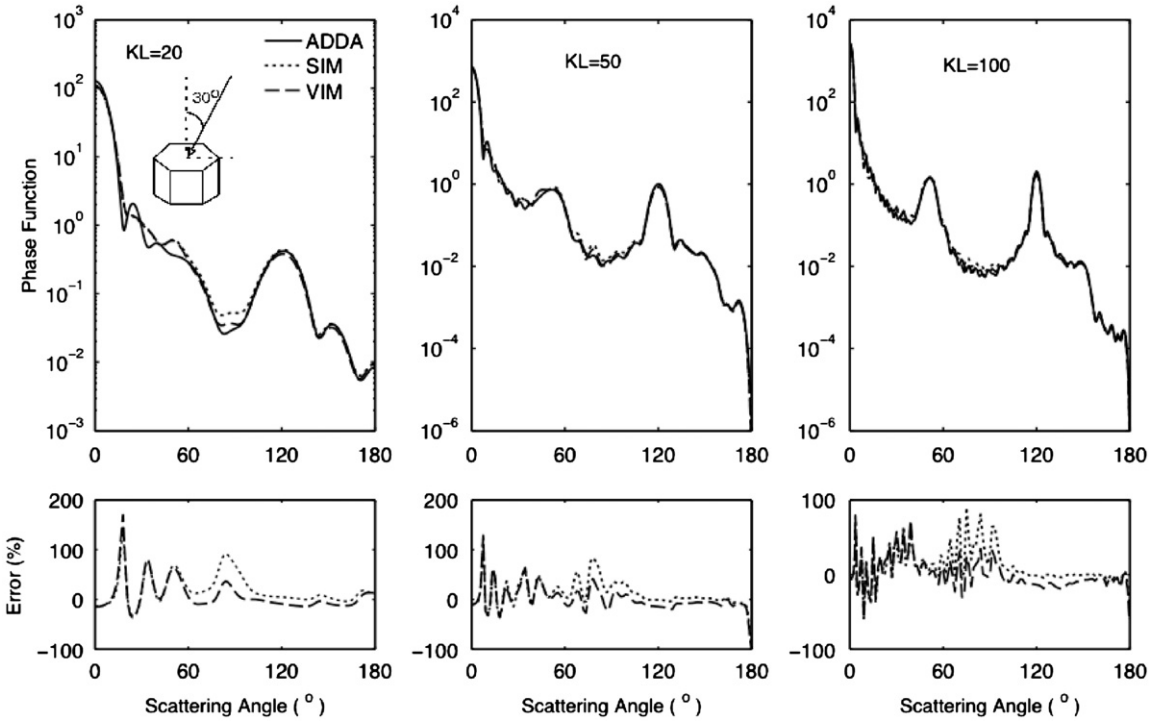

Fig. 4. Same as Fig. 3, except that the incident angle is 30°. The 120° peak is from the top reflection. The 51.3° peak is due to the contributions from two sides. The results are averaged over scattering azimuthal angles.

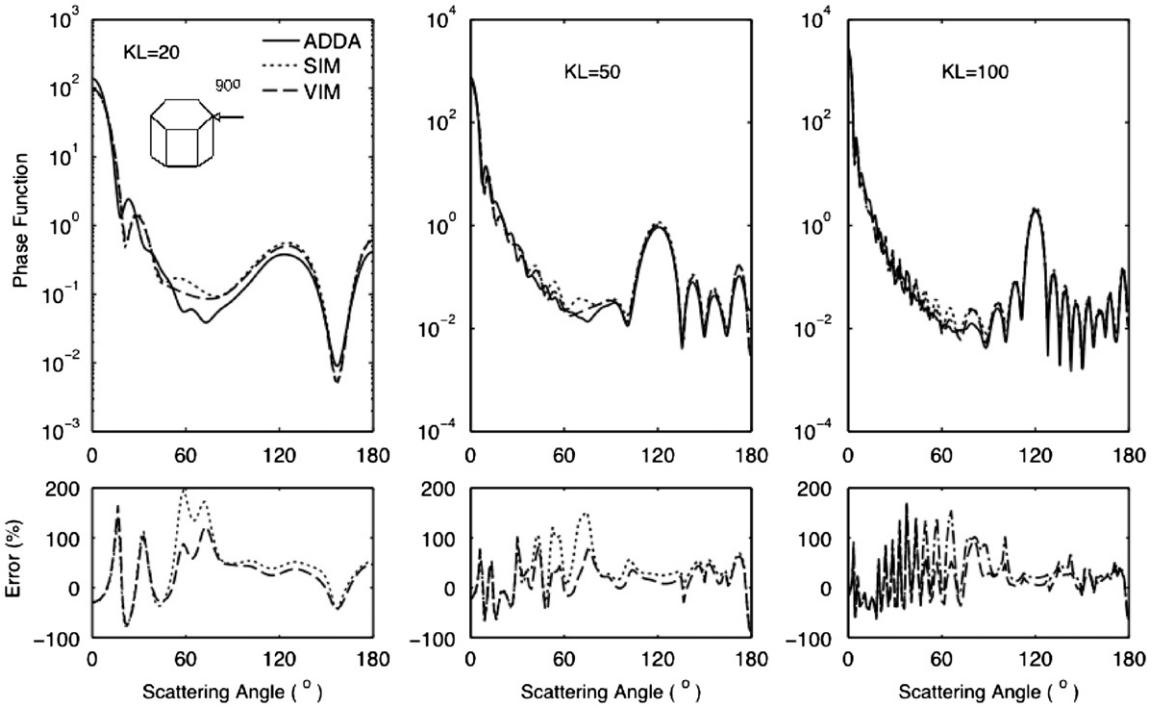

Fig. 5. Same as Fig. 3, except that the incident angle is 90°. The illuminated side is composed of two local planar surfaces. The two scattering angles predicted from ray optics are the same and equal to 120°. The results are averaged over scattering azimuthal angles.

less than 120°. For backscattering angles, the agreement between the methods is better.

In Fig. 4, the direction of the incident light makes an angle of 30° with the axis of the particle and is parallel to one of the mirror planes. Two sharp peaks are found when the size parameter is 100. The 120° peak is associated with the reflection from the top surface while the 51.3° peak is from the reflections from two side faces. When the size parameter decreases, the peaks broaden. At a size parameter of 20, the 51.3° peak is essentially not noticeable. This feature stems from the ray-spreading effect [8,9]. When the incident light is parallel to the top surface, as seen in Fig. 5, the peak arising from the top reflection disappears and the peak location due to the reflection from two side surfaces is at 120°. From the comparison of the phase functions, the difference between the results from the SIM/VIM and the DDA is pronounced when the incident angle of the incoming light is zero. The phase function values at scattering angles larger than 90° are more accurate than those between 0 and 90°. The SIM and the VIM have comparable accuracy, although the formulae are not exactly equivalent.

The difference between the results calculated from the SIM/VIM and the DDA is due to the inaccuracy of the reflected field near the edges. For simplicity, we demonstrate the intensity of the electric field at the top face when the incident angle is 0°, as shown in Fig. 6. The upper and lower panels correspond to the two polarization states of the incident light. In principle, the applicability of ray optics breaks down near the particle edge—the field near the edge is quite different from that within the polygon. At size parameters of 20 and 50, some structures in the intensity pattern may be observed, but these structures become less apparent as the size parameter increases. The comparison shown in Fig. 5 suggests that the edge effect may influence the forward scattering phase function.

Fig. 7(a) shows the comparison of the normalized reflection pattern of randomly oriented hexagonal particles from the ray tracing calculation with the reflection pattern for a sphere with the same refractive index. The general pattern of the external reflection from the ray-tracing technique agrees with that for spheres. However, the ray tracing technique is found to be inaccurate near the forward and the backward directions. From this figure, we can see that the reflection pattern for a sphere can be employed as a proper surrogate for that associated with randomly oriented hexagonal particles. Note that the normalized reflection pattern does not depend on the size parameter of the particle. As discussed in Section 2, the external reflection can also be calculated from the SIM. As shown in Fig. 7(b), the reflection pattern from the SIM depends on the size parameter and is exactly zero in the forward scattering direction. The physical reason for a missing reflection pattern near the forward scattering angle is likely to be associated with the inaccuracy of the reflected field near the boundary of the particle. When the size of the particle is large, the results from the SIM tend to match that of a sphere except the forward scattering. Therefore, a zero reflection in the forward scattering seems to be an artifact. This artifact is not essential in the total phase function as the diffraction dominates in near-forward scattering directions.

For the comparison of the phase function of randomly oriented hexagonal particles from the SIM and the ADDA, shown in Fig. 8(a), the number of orientations was set as

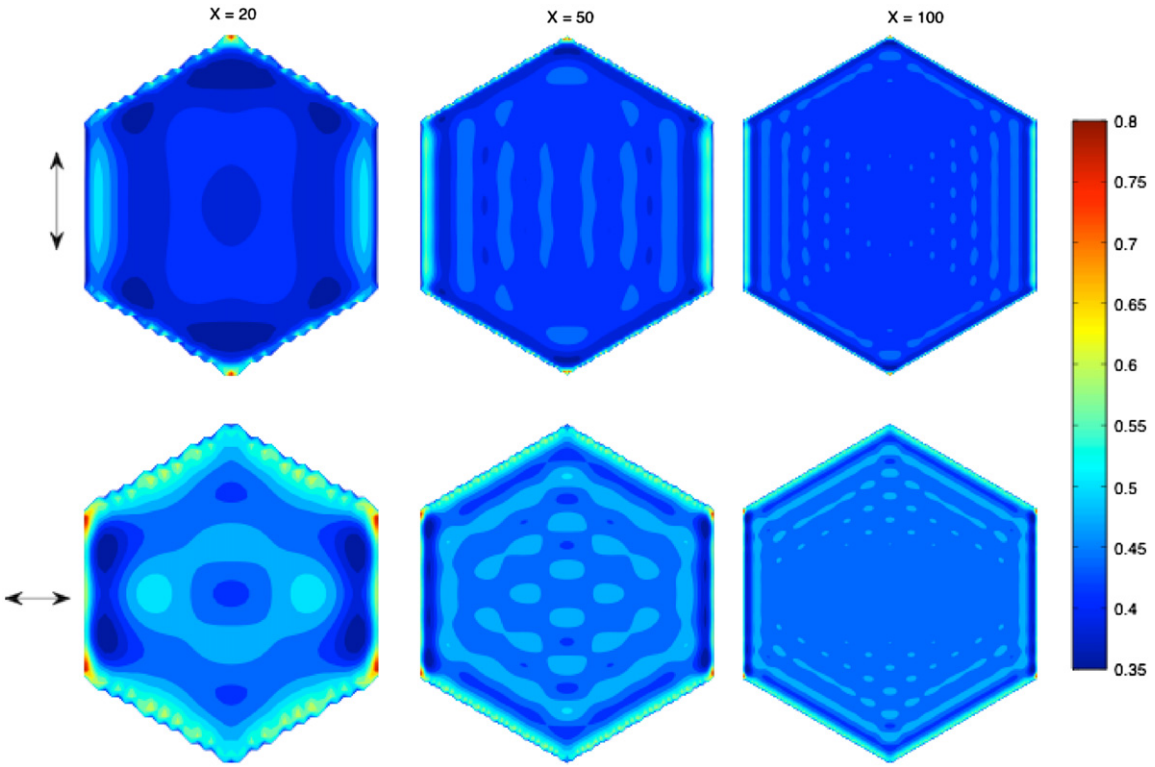

Fig. 6. Intensity of the total field of the first layer of dipoles near the hexagonal top. The direction of incident light is aligned with the axis. The two rows are for different polarization directions of the incident electric field. The three columns correspond to different size parameters.

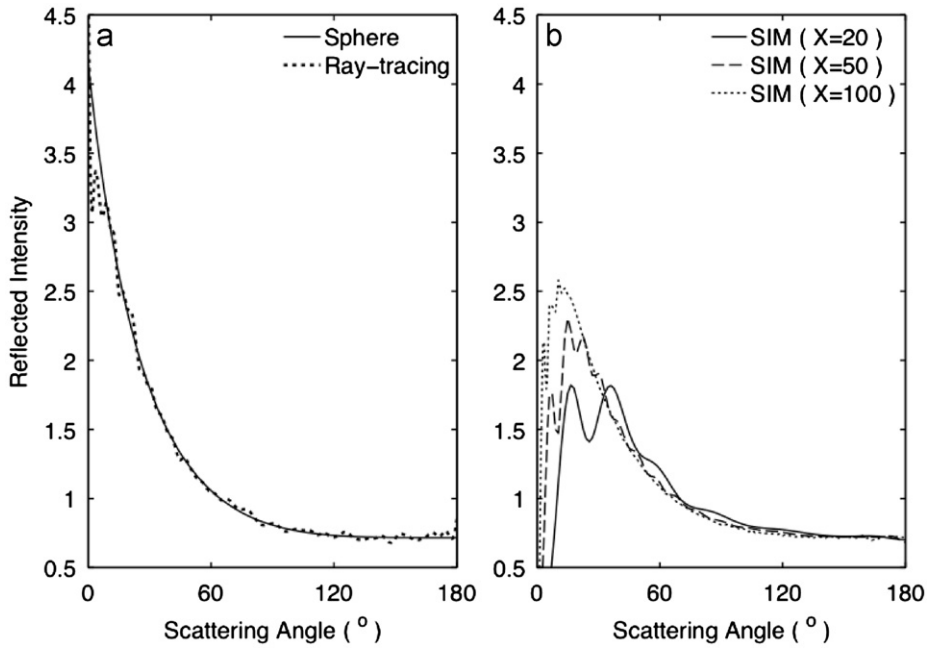

Fig. 7. (a) Comparison of normalized distributions of intensity associated with the external reflection from randomly oriented hexagonal particles calculated from the ray-tracing technique and the analytical solution for spheres with the same refractive index as that of hexagonal particles. (b) Reflection by randomly oriented hexagonal particles calculated from the SIM at three size parameters of 20, 50, and 100.

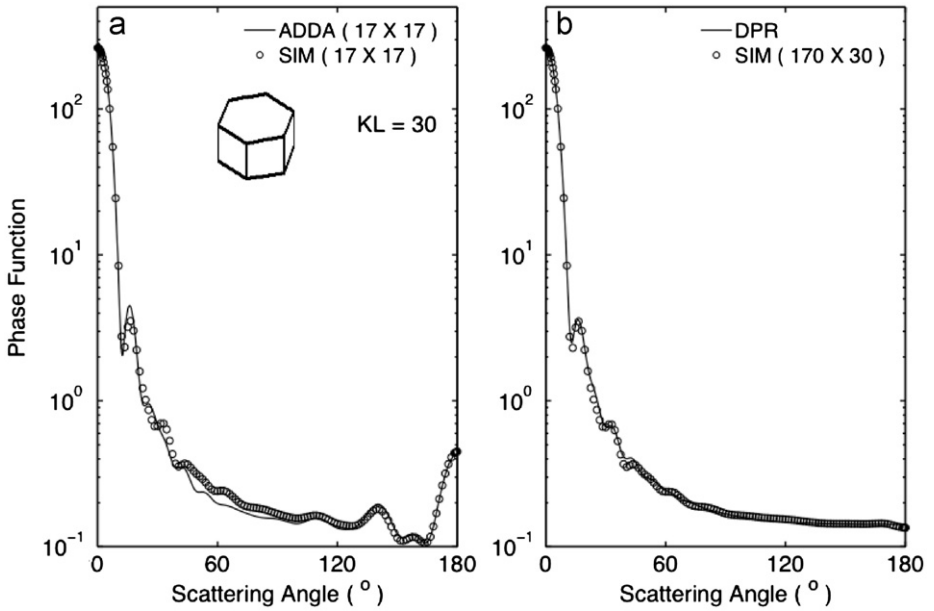

Fig. 8. Comparison of the phase function from the SIM, the ADDA and the DPR for randomly oriented particles. The random orientations in (a) for the ADDA and SIM are set through 17 zenith angles and 17 azimuthal angles. Random orientations in (b) for the SIM are specified through 170 zenith angles and 30 azimuthal angles to produce flat backscattering.

17×17 for the ADDA and SIM simulations. While a close agreement between the SIM and the ADDA is demonstrated, a structure in the backscattering phase function is observed. From the properties of the reflection pattern for randomly oriented particles, the phase function should be flat as illustrated by the DPR method. This is because the number of orientations is insufficient for representing the random orientation condition. Since the ADDA requires more computational time to perform numerical averages over a large number of orientations, we increased the number of orientations for the SIM due to its efficiency. As a result, a flat backscattering feature appears, as shown in Fig. 8(b). Results from the SIM tend to match that of the DPR method, suggesting that the assumptions in the DPR method are reasonable. Therefore, for randomly oriented particles, the DPR method can be used as an efficient method for the first-order scattering simulation without losing accuracy. Note that the DPR is restricted to randomly oriented particles. For particles with preferred orientations, the SIM/VIM should be chosen. This comparison also indicates that the peak in the phase function around 16°, observed in the ADDA calculation, is related to diffraction. For randomly oriented particles with complex shapes, the normalized reflection pattern is not the same as that of a sphere, and then the ray-tracing technique can be used.

4. Summary and conclusions

External reflection and diffraction by hexagonal particles are studied by three approximate methods; the SIM, the VIM and the DPR. The amplitude scattering matrix derived from the SIM and the VIM are not exactly equivalent; however, both have comparable accuracy in a numerical simulation. Comparison of results from the SIM and the VIM with those of the DDA method suggests that the SIM and the VIM are very accurate even for particles with fixed orientations. For randomly oriented hexagonal particles, a flat backscattering feature is validated. The DDA method is insufficient in this case because a large number of random orientations are required that result in a tremendous demand on computational resources. The DPR has proven to be applicable to randomly oriented particles with a reasonable accuracy. Because the diffraction and external reflection can be semi-analytically obtained with a satisfactory accuracy, a standard algorithm can be programmed in a straightforward way.

Acknowledgments

This research is partially supported by a Grant from the National Science Foundation (ATM-0803779). Prof. George W. Kattawar's research is also supported by the Office of Naval Research under contract N00014-06-1-0069.

Appendix A. The calculation of the shape factor D in Eq. (4)

In the present study, the shape factor needs to be calculated with respect to various facets on a particle surface. For simplicity, let the position vector on a local planar face be

$$\vec{r}' = \vec{r}_0 + u\hat{e}_u + v\hat{e}_v, \tag{31}$$

where $\vec{r}_0$ is a given vector of a selected boundary point on the surface, $(\hat{e}_u, \hat{e}_v)$ are two orthogonal unit vectors lying in the surface. Let $\hat{n}$ be along its normal direction. The unit vectors $\hat{e}_u, \hat{e}_v$, and $\hat{n}$ create a local coordinate system. In the new coordinate system, the shape factor is written as

$$D = \frac{k^2}{4\pi}\exp\left\{ik(\hat{e}^i - \hat{r})\cdot\vec{r}_0\right\}\int_s \exp\{ik(\omega_u u + \omega_v v)\}\,du\,dv, \tag{32}$$

where ω_u and ω_v are two defined coefficients, given by

$$\omega_u = (\hat{e}^i - \hat{r})\cdot\hat{e}_u, \quad \omega_v = (\hat{e}^i - \hat{r})\cdot\hat{e}_v. \tag{33}$$

By employing the Stokes theorem [41,42], the integral in Eq. (32) is written as

$$\int_s \exp\{ik(\omega_u u + \omega_v v)\}\,du\,dv = \frac{i}{k^2(\omega_u^2+\omega_v^2)}\int_{\partial s}\exp\{ik(\omega_u u + \omega_v v)\}(\omega_v du - \omega_u dv). \tag{34}$$

For a N-polygon, the integral can be integrated as [41],

$$\int_s \exp\{ik(\omega_u u + \omega_v v)\}\,du dv = \frac{i[\omega_v(u_{i+1}-u_i)-\omega_u(v_{i+1}-v_i)]}{k^2(w_u^2+w_v^2)} \times \exp\{ik[\omega_u(u_{i+1}+u_i)+\omega_v(v_{i+1}+v_i)]/2\} \times \frac{\sin\{k[\omega_u(u_{i+1}-u_i)+\omega_v(v_{i+1}-v_i)]/2\}}{k[\omega_u(u_{i+1}-u_i)+\omega_v(v_{i+1}-v_i)]/2}, \tag{35}$$

Substituting Eq. (35) into Eq. (32) and after some algebra, we obtain

$$D = \frac{ik}{4\pi}\sum_{j=1}^{N}\frac{(\vec{r}_{j+1}-\vec{r}_j)\cdot[(\hat{e}^i-\hat{r})\times\hat{n}]}{|\hat{e}^i-\hat{r}|^2-[(\hat{e}^i-\hat{r})\cdot\hat{n}]^2}\,\frac{\sin\{k(\hat{e}^i-\hat{r})\cdot(\vec{r}_{i+1}-\vec{r}_i)/2\}}{k(\hat{e}^i-\hat{r})\cdot(\vec{r}_{i+1}-\vec{r}_i)/2} \times\exp\{ik(\hat{e}^i-\hat{r})\cdot(\vec{r}_{i+1}+\vec{r}_i)/2\}. \tag{36}$$

Note that in Eq. (36) the sequence of vertices is in a counterclockwise direction, $\vec{r}_{N+1} = \vec{r}_1$, and the normal direction is facing the incident wave. Calculation of Eq. (36) can be done in an arbitrary 3-D space.

Appendix B. Diffraction by a regular hexahedron

In a general formulation, the amplitude scattering matrix associated with the diffraction by a 3-D facet is given by,

$$S_{11}^d = -D[(1+\cos\theta)\hat{e}_i\cdot\hat{n} + \sin\theta\sin\phi\hat{\alpha}_i\cdot\hat{n} + \sin\theta\cos\phi\hat{\beta}_i\cdot\hat{n}]. \tag{37}$$

$$S_{12}^d = D(\sin\theta\cos\phi\hat{\alpha}_i\cdot\hat{n} - \sin\theta\sin\phi\hat{\beta}_i\cdot\hat{n}), \tag{38}$$

$$S_{21}^d = -S_{12}^d, \quad S_{22}^d = S_{11}^d. \tag{39}$$

where $\hat{n}$ is the outward normal direction of the facet, $\hat{e}_i$ is the direction of incident light, $\hat{\alpha}_i$ and $\hat{\beta}_i$ are two polarization vectors, and θ and ϕ are the scattering angle and the azimuthal angle of scattering plane. When the incident light is normally impinging on the bottom of a regular hexahedron, as shown in Fig. 9, it can be proved that

$$S_{top}^d = -\begin{bmatrix}1+\cos\theta & 0\\ 0 & 1+\cos\theta\end{bmatrix} ab\frac{\sin(ka\omega_x)}{ka\omega_x}\frac{\sin(kb\omega_y)}{kb\omega_y}\exp(ikc\omega_z), \tag{40}$$

$$S_{bottom}^d = \begin{bmatrix}1+\cos\theta & 0\\ 0 & 1+\cos\theta\end{bmatrix} ab\frac{\sin(ka\omega_x)}{ka\omega_x}\frac{\sin(kb\omega_y)}{kb\omega_y}\exp(-ikc\omega_z), \tag{41}$$

$$S_{left}^d = \begin{bmatrix}\sin\phi & -\cos\phi\\ \cos\phi & \sin\phi\end{bmatrix}\sin\theta ac\frac{\sin(ka\omega_x)}{ka\omega_x}\frac{\sin(kc\omega_z)}{kc\omega_z}\exp(-ikb\omega_y), \tag{42}$$

$$S_{right}^d = -\begin{bmatrix}\sin\phi & -\cos\phi\\ \cos\phi & \sin\phi\end{bmatrix}\sin\theta ac\frac{\sin(ka\omega_x)}{ka\omega_x}\frac{\sin(kc\omega_z)}{kc\omega_z}\exp(kb\omega_y), \tag{43}$$

$$S_{front}^d = -\begin{bmatrix}\cos\phi & \sin\phi\\ -\sin\phi & \cos\phi\end{bmatrix}\sin\theta bc\frac{\sin(kb\omega_y)}{kb\omega_y}\frac{\sin(kc\omega_z)}{kc\omega_z}\exp(ika\omega_x), \tag{44}$$

$$S_{back}^d = \begin{bmatrix}\cos\phi & \sin\phi\\ -\sin\phi & \cos\phi\end{bmatrix}\sin\theta bc\frac{\sin(kb\omega_y)}{kb\omega_y}\frac{\sin(kc\omega_z)}{kc\omega_z}\exp(-ika\omega_x). \tag{45}$$

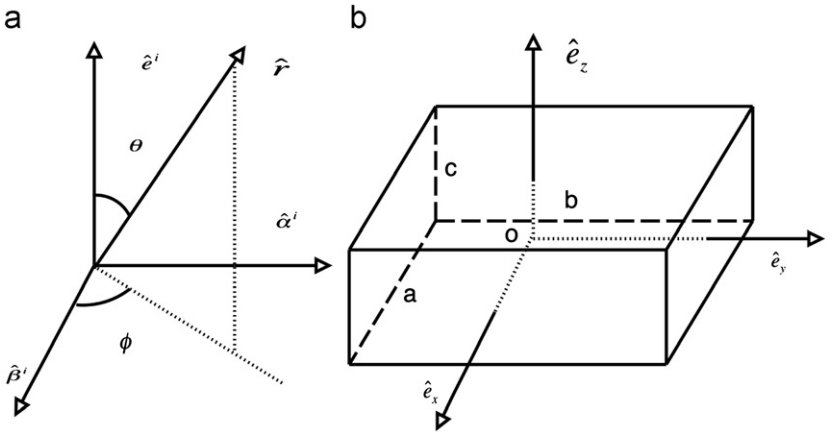

Fig. 9. Schematic geometry of diffraction by a regular hexahedron.

where ω_x, ω_y, and ω_z are three components of vector $\vec{\omega} = (\hat{e}^i - \hat{r})/2$. Note that S^d_{top} and S^d_{bottom} have a phase difference. It can be shown that $S^d_{bottom} + S^d_{left} + S^d_{right} + S^d_{front} + S^d_{back} = -S^d_{top}$.

References

[1] van de Hulst HC. Light scattering by small particles. New York: Wiley; 1957.
[2] Nussenzveig HM. Diffraction effects in semiclassical scattering. Cambridge, UK: Cambridge University Press; 1992.
[3] Jacobowitz H. A method for computing the transfer of solar radiation through clouds of hexagonal ice crystals. JQSRT 1971;11:691–5.
[4] Wendling P, Wendling R, Weickmann HK. Scattering of solar radiation by hexagonal ice crystals. Appl Opt 1979;18:2663–71.
[5] Cai Q, Liou KN. Polarized light scattering by hexagonal ice crystals: theory. Appl Opt 1982;21:3569–80.
[6] Takano Y, Jayaweera K. Scattering phase matrix for hexagonal ice crystals computed from ray optics. Appl Opt 1985;24:3254–63.
[7] Macke A. Scattering of light by polyhedral ice crystals. Appl Opt 1993;32:2780–8.
[8] Muinonen K. Scattering of light by crystals: a modified Kirchhoff approximation. Appl Opt 1989;28:3044–50.
[9] Yang P, Liou KN. Geometric-optics-integral-equation method for light scattering by nonspherical ice crystals. Appl Opt 1996;35:6568–84.
[10] Yang P, Liou KN. Light scattering by hexagonal ice crystals: solutions by a ray-by-ray integration algorithm. J Opt Soc Am A 1997;14:2278–89.
[11] Yang P, Liou KN. Single-scattering properties of complex ice crystals in terrestrial atmosphere. Contrib Atmos Phys 1998;71:223–48.
[12] Zhang Z, Yang P, Kattawar GW, Tsay SC, Baum BA, Hu Y, et al. Geometrical-optics solution to light scattering by droxtal ice crystals. Appl Opt 2004;43:2490–9.
[13] Yang P, Wei HL, Huang HL, Baum BA, Hu Y, Kattawar GW, et al. Scattering and absorption property database for nonspherical ice particles in the near-through far-infrared spectral region. Appl Opt 2005;44:5512–23.
[14] Zhang Z, Yang P, Kattawar GW, Wiscombe WJ. Single-scattering properties of platonic solids in geometrical-optics regime. JQSRT 2007;106:595–603.
[15] Dubovik O, Holben BN, Lapyonok T, Sinyuk A, Mishchenko MI, Yang P, et al. Non-spherical aerosol retrieval method employing light scattering by spheroids. Geophys Res Lett 2002;29:45, doi:10.1029/2001GL014506.
[16] Yang P, Feng Q, Hong G, Kattawar GW, Wiscombe WJ, Mishchenko MI, et al. Modeling of the scattering and radiative properties of nonspherical dust particles. J Aerosol Sci 2007;38:995–1014.
[17] Bi L, Yang P, Kattawar GW, Kahn R. Single-scattering properties of triaxial ellipsoidal particles for a size parameter range from the Rayleigh to geometric-optics regimes. Appl Opt 2009;48:114–26.
[18] Takano Y, Liou KN. Solar radiative transfer in cirrus clouds, I, single-scattering and optical properties of hexagonal ice crystals. J Atmos Sci 1989;46:3–19.
[19] Mishchenko MI, Macke A. Incorporation of physical optics effects and computation of the Legendre expansion for ray-tracing scattering functions involving δ-function transmission. J Geophys Res 1998;103:17991805.
[20] Yang P, Liou KN. Light scattering and absorption by nonspherical ice crystals. In: Kokhanovsky AA, editor. Light scattering reviews: single and multiple light scattering. Chichester, UK: Springer-Praxis; 2006. p. 31–71.
[21] Borovoi AG, Grishin IA. Scattering matrices for large ice crystal particles. J Opt Soc Am A 2003;20:2071–80.
[22] Hesse E, Ulanowski Z. Scattering from long prisms computed using ray tracing combined with diffraction on facets. JQSRT 2003;79:721–732.
[23] Clarke JM, Hesse E, Ulanowski Z, Kaye PH. A 3D implementation of ray tracing combined with diffraction on facets: Verification and a potential application. JQSRT 2006;100:103–14.
[24] Hesse E. Modelling diffraction during ray tracing using the concept of energy flow lines. JQSRT 2008;109:1374–83.
[25] Hovenac EA, Lock JA. Assessing the contributions of surface waves and complex rays to far-field Mie scattering by use of the Debye series. J Opt Soc Am A 1992;9:781–95.
[26] Yang P, Gao BC, Baum BA, Wiscombe WJ, Mischenko MI, Winker DM, et al. Asymptotic solutions of optical properties of large particles with strong absorption. Appl Opt 2001;40:1532–47.
[27] Lock JA. Ray scattering by an arbitrarily oriented spheroid. I. Diffraction and specular reflection. Appl Opt 1996;35:500–14.
[28] Yee SK. Numerical solution of initial boundary value problems involving Maxwell's equations in isotropic media. IEEE Trans Antennas Propag 1966;14:302–7.
[29] Yang P, Liou KN. Finite-difference time domain method for light scattering by small ice crystals in three-dimensional space. J Opt Soc Am 1996;A13:2072–85.
[30] Sun W, Fu Q, Chen Z. Finite-difference time-domain solution of light scattering by dielectric particles with perfectly matched layer absorbing boundary conditions. Appl Opt 1999;38:3141–51.
[31] Purcell EM, Pennypacker CR. Scattering and absorption of light by nonspherical dielectric grains. Astrophys J 1973;186:705–14.
[32] Draine BT. The discrete-dipole approximation and its application to interstellar graphite grains. Astrophys J 1988;333:848–72.
[33] Goedecke GH, O'Brien SG. Scattering by irregular inhomogeneous particles via the digitized Green's function algorithm. Appl Opt 1988;27:2431–8.
[34] Yurkin MA, Maltsev VP, Hoekstra AG. The discrete dipole approximation for simulation of light scattering by particles much larger than the wavelength. JQSRT 2007;106:546–57.
[35] Waterman PC. Matrix formulation of electromagnetic scattering. Proc IEEE 1965;53:805–12.
[36] Mishchenko MI, Travis LD, Mackowski DW. T-matrix computations of light scattering by nonspherical particles: a review. JQSRT 1996;55:535–75.
[37] Doicu A, Eremin Y, Wriedt T. Acoustic and electromagnetic scattering analysis using discrete sources. New York: Academic Press; 2000.
[38] Havemann S, Baran AJ. Extension of T-matrix to scattering of electromagnetic plane waves by non-axisymmetric dielectric particles: application to hexagonal ice cylinders. JQSRT 2001;70:139–158.
[39] Jackson JD. Classical electrodynamics, 3rd ed. New York: Academic Press; 1998.
[40] Saxon DS. Lectures on the scattering of light. Los Angeles: University of California; 1955.
[41] Gordon W. Far-field approximations to the Kirchhoff–Helmholtz representations of scattered fields. IEEE Trans Antennas Propag 1975;23:590–2.
[42] Heffels C, Heitzmann D, Hirleman ED, Scarlett B. Forward light scattering for arbitrary sharp-edged convex crystals in Fraunhofer and anomalous diffraction approximations. Appl Opt 1995;34:6552–6560.